Waste and Biomass Valorization (2023) 14:3893–3907
https://doi.org/10.1007/s12649-023-02105-8

ORIGINAL PAPER

Valorization of Primary Sludge and Biosludge from the Pulp Mill Industry in Uruguay Through Hydrothermal Carbonization

Mirian Elizabeth Casco[1] · Valentín Moreno[1] · Martín Duarte[1] · Karim Sapag[2] · Andrés Cuña[3]

Received: 10 November 2022 / Accepted: 27 February 2023 / Published online: 16 March 2023

Abstract

Although nowadays landspreading and incineration are the conventional disposal methods for the primary sludge (PS) and biosludge (BS) generated in the wastewater treatment plants of the pulp mill industry in Uruguay, their direct incineration for energy recovery is the most preferable one. Here, we propose the hydrothermal carbonization (HTC) method as a pre-treatment to improve the fuel characteristic of PS and BS. Proximate and ultimate analysis, scanning electron microscopy, and thermogravimetric analysis show that the HTC affects PS and BS differently regarding carbon fixation, energy densification and energy conversion efficiency. Moreover, ash composition measured by X-ray fluorescence indicates that the HTC effectively diminishes the slagging and fouling indexes for both feedstocks, which can increase the life expectancy of boilers. Alternative PS, BS, and their hydrochars were activated with H_3PO_4 to produce activated carbons, i.e. the BET specific surface area was as high as 800 m^2/g for PS-AC, and exhibits CO_2 adsorption capacity of 5 mmol/g at 10 bar at 273 K. These studies provide alternatives to direct incineration and landspreading of PS and BS in Uruguay to reduce their environmental impact, either by enhancing their fuel quality or by converting them into much more valuable products to face air pollution.

Graphical Abstract

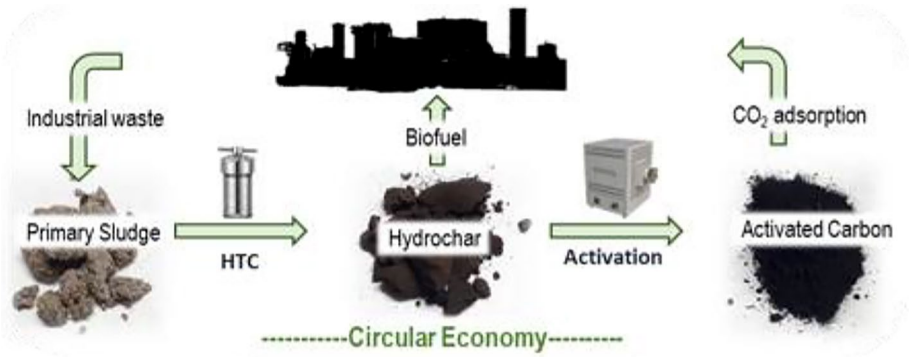

Keywords Valorization · Sludge · Biofuel · Activated carbon · CO_2 adsorption

✉ Mirian Elizabeth Casco
mirian.casco@ucu.edu.uy

[1] Departamento de Ingeniería, Universidad Católica del Uruguay, Av. 8 de Octubre 2738, CP 11600 Montevideo, Uruguay

[2] Laboratorio de Sólidos Porosos, INFAP, CONICET-Universidad Nacional de San Luis, Ejército de los Andes 950, San Luis, Argentina

[3] Área Fisicoquímica, DETEMA, Facultad de Química, Universidad de la República, Av. General Flores 2124, CP 11800 Montevideo, Uruguay

Statement of Novelty

The paper focuses on a hydrothermal approach as pre-treatment to improve the fuel quality of two residues from the wastewater treatment plant of the pulp mill industry in Uruguay. It includes the analysis of the different response of both feedstocks based on their unique nature. Alternatively, the paper proposes the preparation of low-cost activated

carbons immobilizing inorganic material and their performance as CO_2 adsorbents.

Introduction

Worldwide, the demand for cellulose continues to grow steadily, being Uruguay an attractive location for cellulose pulp companies looking for price and quality in their products. Currently, two pulp industries operate in Uruguay, UPM and Montes del Plata. Both use the chemical Kraft process to produce approximately 1.3 MADt[1] of fully bleached Eucalyptus pulp per year each [1, 2]. The main drivers for investments in the region are the availability, fast growth rate, and good quality of Eucalyptus wood, together with a legal framework for the promotion of the free trade zone regime[2] and the forest law.[3] In this context, a second pulp mill industry is being built by UPM company in the center of the country (Paso de los Toros city) with a higher production capacity of 2.1 MADt per year with the possibility of increasing it by 11% [3].

During the processing of Eucalyptus fibers to obtain cellulose, large amounts of solid waste are generated, mainly in the form of sludge from the wastewater treatment plant (WWTP). For instance, the effluents generated in the UPM Fray Bentos pulp mill (mainly from the bleaching process) are treated in a WWTP composed of a conventional activated sludge system with an installed capacity to treat approximately 73,000 m^3/day [4]. The sludge settled out in the primary sedimentation tank (primary sludge), composed mainly of fibers and suspended solid, is dewatered in two screw filter presses with a total capacity of 33.8 total dry solids (t DS)/d. Similarly, the activated sludge from the secondary sedimentation tank (biosludge) is treated in a gravity table and a decanter centrifuge with a capacity of 17 t DS/d. Then, dewatered biosludge is dried in two biosludge bed dryers with steam moisture less than 10%. Currently, it generates 30,000 t/year on wet basis (60–80% humidity) of primary sludge and around 10,000 t/year on wet basis (95% humidity) of biosludge [5]. After dewatering, primary sludge and biosludge are transported to their final disposal site in landspreading (in forest plantations).

On the other hand, the forestry activity represents 3.8% of the GDP in Uruguay. Therefore, to assure the sector's long-term productivity, it is crucial to mitigate the environmental impact caused by their residues. In this line, responsible waste management is one of the commitments of companies in Uruguay, reflected in the goal "zero waste to landfill to 2030". An industrial fluidized bed biomass boiler to incinerate WWTP sludge is a short-term solution for this problem. Nonetheless, this option suffers from weak economics due to the need for sludge dewatering or energy-intensive evaporation in the recovery boilers, apart from environmental concerns such as atmospheric emissions and ash disposal [5]. Therefore, evaluating other valorization technologies apart from energy recovery by incineration is on the company's agenda [6].

Hydrothermal carbonization (HTC) technology is an attractive pretreatment alternative to the direct incineration of biomass and biomass waste [5]. Despite its almost one hundred years, the HTC method has become more significant in recent years because it is relatively simple and environmentally friendly. It involves the thermal treatment of wet feedstock under autogenously generated subcritical water pressure. Usually, the reaction occurs in an autoclave under mild conditions, that is, at 180–250 ºC and 2–3 MPa for several hours. Thereby the organic materials can be converted into carbon-rich solid materials with higher calorific value, involving low operational cost.

The HTC method is desirable as a pretreatment solution in managing primary sludge (PS) and biosludge (BS). During the HTC process of biomass, a series of decomposition reactions such as dehydration, and decarboxylation happen with the consequent release of water and carbon dioxide from the feedstock's structure while fixing the carbon in an easily separable solid phase, denoted as hydrochar [7, 8]. After treatment, the initial volume of solid waste is considerably reduced, as well as its potential toxicity. In addition, the hydrochar can be easily pelletized to be stored and used on demand, for soil amendment, biofuel, or as a precursor to producing activated carbons [9, 10]. In the literature, the production of activated carbon using hydrochars from several wet feedstocks (e.g., sewage sludge, paper sludge, organic waste, biomass waste) has received increasing attention due to the wide range of applications of this material, such as environmental remediation and energy storage [9–12].

Since the differences in chemical compositions (the nature of the organic fraction and ash composition) among the various paper and pulp sludge result in divergences in the resulting hydrochar [12–14], and the incineration of the PS and BS from the bleached Eucalyptus Kraft pulp mill in Uruguay is imminent; the first goal of this work is to evaluate the effect of the hydrothermal treatment on the fuel characteristic of these residues. A second objective is to evaluate the valorization of PS and BS and their resulting hydrochars, utilizing them as activated carbon precursors for CO_2 adsorption applications.

[1] *ADt: air dry ton.*

[2] *Ley 15.921 del 17 de diciembre de 1987, y su Decreto Reglamentario 454/88 del 8 de julio de 1988,*

[3] *Ley 15.939 del 28 de diciembre de 1987 y modificativas, y su Decreto reglamentario 452/88 del 6 de julio de 1988 y modificativos.*

Table 1 Experimental conditions and sample code

	190 °C	220 °C
	PS	
2 h	190PS2	220PS2
12 h	190PS12	220PS12
24 h	190PS24	220PS24
	BS	
2 h	190BS2	220BS2
12 h	190BS12	220BS12
24 h	190BS24	220BS24

Materials and Methods

Raw Materials

The primary clarifier sludge, primary sludge (PS), and the secondary clarifier sludge, biosludge (BS) were supplied by an Uruguayan pulp industry (Fig. S1). BS was dried in the WWTP before being sent to the laboratory and a moisture of 5.7% remains. PS was received with moisture of 69.3%.

Hydrothermal Carbonization (HTC) Experiments

The hydrothermal carbonization experiments were performed using 60 g of total mass (sludge + water) in a 250 ml stainless steel hydrothermal autoclave with a PTFE inner chamber. The BS was humidified with distilled water up to 75% of moisture, while PS was used as received, with a moisture of 69.3%. Table 1 summarizes the experimental conditions. After the treatment, the reactor was cooled down, the solid was filtered under vacuum, dried in an oven overnight at 105ºC, and weighted for mass balance calculation.

Proximate Analysis

The PS and BS and all hydrochars were analyzed for moisture, volatile matter (VM), fixed carbon (FC) and ash content (ASH). Moisture was calculated by the difference between the sample weight before and after being exposed overnight at 105 ºC in an oven. The VM and ASH were tested according to the protocol ASTM D 3172–3175. The FC was calculated on dry basis according to Eq. (1):

$$FC = 100 - VM - ASH \quad (1)$$

Hydrochars 220PS24 and 220BS12 were selected to analyze their fuel characteristics and, as precursors to produce activated carbons. The morphology of the raw materials and the selected hydrochars was characterized by scanning electron microscopy (SEM) with a JEOL JSM-5900LV equipment under 20 kV of the voltage supply. The elemental composition of different zones was made with an Energy Dispersive Spectrometer probe (Thermo Noran system 7).

Liquid Fraction Analysis

Analytical parameters for the liquid fraction obtained after HTC experiments such as total chemical oxygen demand (COD), total nitrogen (TN), total phosphorus (TP), and total suspended solids (TSS) were determined according to the standard methods 5220-D, DIN EN ISO 11905-1, 4500-P E and 2540D, respectively [13]. A spectrometer Spectroquant® Prove 300 and a digestor Spectroquant® TR 320 were used for the determination.

Ultimate Analysis

The PS, BS, 220PS24, and 220BS2 were dry at 105 °C prior to ultimate analysis. The elemental components quantification, including hydrogen (H), carbon (C), nitrogen (N), and sulfur (S), was performed with CHNS/O Thermo Scientific FLASH 2000 instruments. Oxygen (O) was determined by difference (O% = 100%–C%–N%–H%–S%–ASH).

The High Heating Value (HHV) was determined following the protocol ASTM D5865 with a Calorimetric bomb, model Parr 1341, equipped with a 6672 precision thermometer. The determination was performed with 0.5 g of sample. For each determination, the correction for the heat of the acid formation was applied according to the calorimetric bomb manual.

Determination of Combustion Indexes

Thermogravimetric analysis (TG) was performed using a SHIMADZU TGA-50 thermal analyzer at heating rates of 5 °C/min with temperatures ranging from room temperature (*ca.* 20–25 °C) to 900 °C. Compressed air was used for combustion experiments at 50 mL/min. About 2.5 ± 0.2 mg sample was weighed and placed in a platinum crucible.

The TG and DTG (derivative thermogravimetric) curves allow identifying different combustion temperatures and combustion indexes. The ignition temperature (T_i) represents the temperature at which the sample starts to burn, determined by the TG-DTG intersection method [15]. The maximum peak temperature (T_p) represents the temperature corresponding to the peak of the DTG profile. The burnout temperature (T_b) represents the point at which mass stabilization occurs [16]. The combustion indexes are the ignition index (D_i), the burnout index (D_b), the combustion index (S),

and the combustion stability index (H_f). They are calculated using Eq. (2–5) [17].

$$D_i = \frac{DTG_{max}}{t_P \cdot t_i} \tag{2}$$

$$D_b = \frac{DTG_{max}}{t_{0.5} \cdot t_b \cdot t_i} \tag{3}$$

$$S = \frac{DTG_{max} \cdot DTG_{mean}}{T_i^2 \cdot T_b} \tag{4}$$

$$H_f = T_p \cdot \ln\left(\frac{t_{0.5}}{DTG_{mean}}\right) \times 10^{-3} \tag{5}$$

where *DTG* max is the maximum combustion rate expressed in wt%/min, DTG_{mean} is the mean combustion rate expressed in wt%/min, t_p is the maximum peak time in min, t_i is the ignition time in min, and $t_{0.5}$ is the time range of $DTG/DTG_{max} = 0.5$ in min.

Determination of Slagging and Fouling Indexes

The quantitative elemental composition analysis of the combustion ash of PS, BS, 220PS24, and 220BS2 was measured by X-ray fluoresce (XRF) technique using a Niton XL2 XRF ThermoFisher Scientific analyzer in mining mode. The elements found in ash are reported as the weight percentage of their stable oxides, such as $SiO_2, Al_2O_3, TiO_2, Fe_2O_3, CaO, MgO, Na_2O, K_2O, P_2O_5$, SO_3. The basic to-acid ratio ($R_{B/A}$) is calculated by Eq. (6) [18, 19]:

$$\mathrm{R_{B/A}} = \left(\frac{\mathrm{Fe_2O_3 + CaO + MgO + Na_2O + K_2O + P_2O_5}}{\mathrm{SiO_2 + Al_2O_3 + TiO_2}}\right) \tag{6}$$

The Slagging index (R_S) is calculated using Eq. (7):

$$R_S = R_{B/A} \cdot S^d \tag{7}$$

where S^d is the percentage of sulfur in dry basis in the solid fuel.

The Fouling index (F_u) is calculated using Eq. (8)

$$F_u = R_{B/A} \cdot \left(Na_2O + K_2O\right) \tag{8}$$

Activated Carbon Synthesis and Characterization

Hydrochars 220PS24 and 220BS2 were selected as activated carbon precursors since they showed the highest FC content. The precursors were impregnated with a 44 wt% solution of phosphoric acid (1 g of precursor for 2 ml of solution) at boiling point for 1 h. Afterward, the impregnated precursor was placed in an oven at 105 ℃ overnight for drying. Next, the sample was heat treated in a tubular horizontal furnace (SNOL company) under a flow of 100 ml/min (heating rate 2 ℃/min) at 450 ℃ for 2 h. Finally, the sample was washed with distilled water to removed other reaction products and dry overnight in an oven at 105 ℃. The hydrochars-derived activated carbons were labeled 220PS24-AC and 220BS24-AC, where AC is referred to as activated carbon.

The nitrogen adsorption/desorption isotherms at 77 K were carried out using an ASAP 2000 sorption analyzer from Micromeritics. Before any measurement, the samples were degassed at 423 K for 12 h. First, the specific surface area (SSA_{BET}) was calculated using the equation from Brunauer–Emmett–Teller (BET) in the range that fits to the consistency criteria proposed by Rouquerol and Llewellyn [20]. Next, the total pore volume ($V_{t,0.9}$) was calculated at a relative pressure of 0.90, according to the Gurvich rule, and the microporosity by applying the Dubinin-Radushkevich equation ($V_{N2,DR}$). The difference between $V_{t,0.9}$ and $V_{N2,DR}$ is considered as the mesopore volume (V_{meso}). Finally, pore size distribution was calculated by applying the Quenched-Solid Density Functional Theory (slit pore, QSDFT equilibrium model) to the nitrogen adsorption isotherm data.

CO_2 adsorption data at 273 K were obtained using an ASAP 2050 sorption analyzer from Micromeritics. Before to any measurement, the samples were degassed at 423 K for 12 h. Then, the microporosity was calculated by applying the Dubinin-Radushkevich equation ($V_{CO2,DR}$), and the micropore size distributions were evaluated by the modified Horvath-Kawazoe method for pores with slit geometries [19, 20].

Isosteric Heat of CO_2 Adsorption

The isosteric heat of adsorption (Q_{st}) in Kj/mol was calculated by applying the Clausius–Clapeyron approach [21] Eq. (9), to CO_2 adsorption isotherms using three temperatures, 273 K, 298 K and 323 K.

$$Q_{st} = R \cdot \left[\frac{\partial lnp}{\partial(1/T)}\right]_{n_{ads}} \tag{9}$$

where p is the equilibrium pressure in kPa, T is the temperature of adsorption in K and R is the universal gas constant, 8.314 kJ/mol/K. The equilibrium pressure (p) for each CO_2 amount adsorbed (n_{ads}) where estimated using a non-linear interpolation from the data of the experimental isotherms at the three temperatures (273, 298, and 323 K). The slope of the straight line of the adsorption isosthere (*ln p* versus *1/T*) corresponds to the isosteric heat of CO_2 adsorption for a defined CO_2 amount adsorbed.

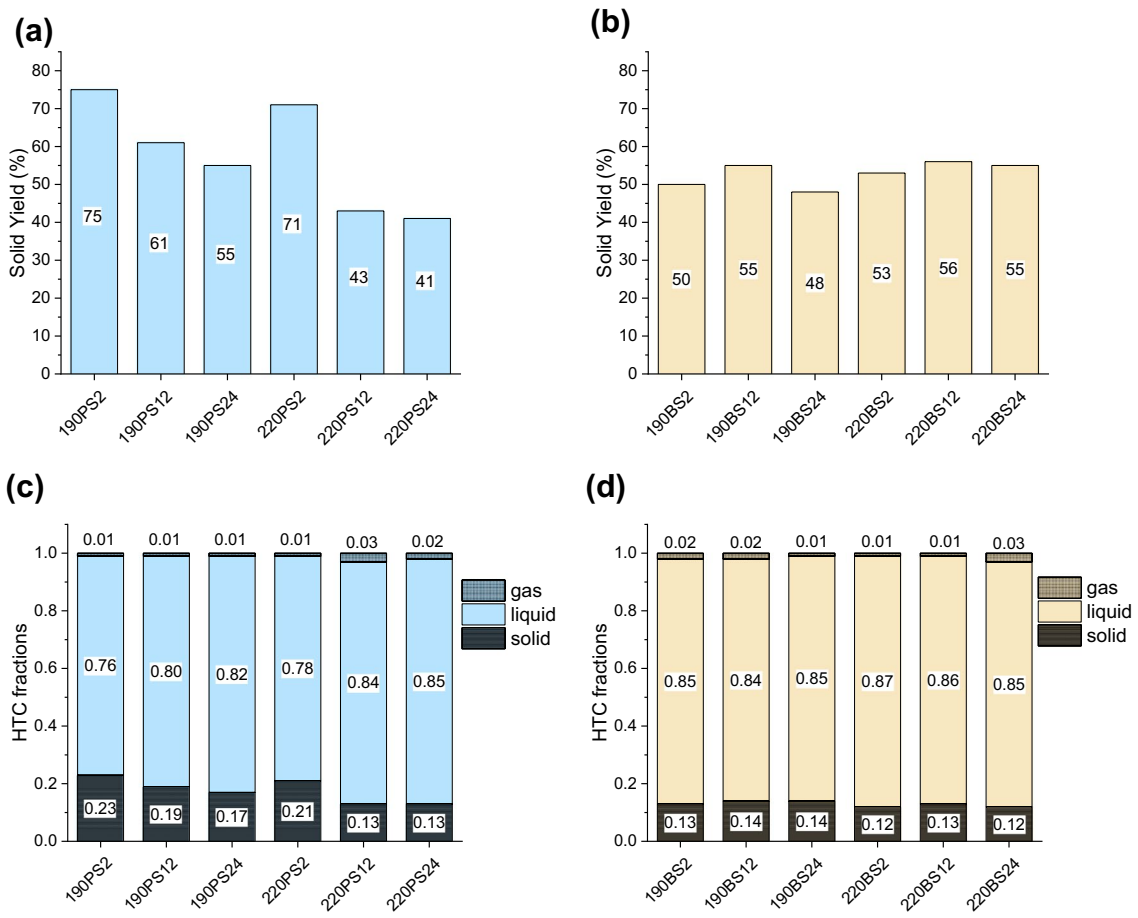

Fig. 1 Solid yield (%) on dry basis for **a** Primary sludge and, **b** Biosludge. Mass balance expressed as HTC fractions (gas, liquid and solid) for **c** Primary sludge and, **d** Biosludge

Results and Discussions

Hydrothermal Carbonization (HTC)

The studied HTC parameters, such as reaction temperature (190 and 220 ℃) and residence time (2, 12, 24 h), have a strong influence on the evolution of the solid yield for the primary sludge (PS), although not for the biosludge (BS). For PS, the yield has a clear downward tendency, from 75 to 41%, as the reaction conditions become severe (Fig. 1a). In contrast, this value is already small at the less severe condition (190 ℃ and 2 h) for BS, and oscillates between 48 to 56% (Fig. 1b). The mass balance (Fig. 1c, d) shows that only a minor fraction of gas is formed (0.01–0.03) for both feedstocks, while the liquid fraction is the highest. The latter varies in a range of 0.76–0.86 for PS. The solid fraction varies oppositely in the range of 0.13–0.23, following a similar tendency as the solid yield. In the case of BS, the liquid, and solid fractions barely change with reaction conditions (0.84–0.87 and 0.12–0.14, respectively). Overall, these results anticipate a lower hydrothermal reaction resistance of the BS than the PS (note that the yield is 50% for BS and 72% for PS at the less severe HTC conditions), likely due to their different chemical nature: PS originates in the so-called 'fiber effluent' of the industrial process (biomass rich in cellulose, hemicellulose, and lignin) and BS in the active sludge reactor (biomass mainly composed of microorganisms, bacteria, and protozoa) [22]. Previous reports where HTC was applied to sewage sludge (composition similar to BS) showed that early liquefaction is promoted at 150 ºC due to the solubilization of small organic compounds and decomposition of the nitrogen compounds from proteins [23, 24].

The proximate analysis provides further information about biomass waste transformation after the hydrothermal treatment. It determines the percentage of fixed carbon (FC), volatile matter (VM), and inorganic compounds (Ash) on dry basis. The results follow a similar tendency for both feedstocks when increasing the reaction severity: an increase of the fixed carbon, a reduction of the volatile matter, and a rise in the ash content (Fig. 2). Nonetheless, the reaction conditions affect the PS and BS transformation and carbon

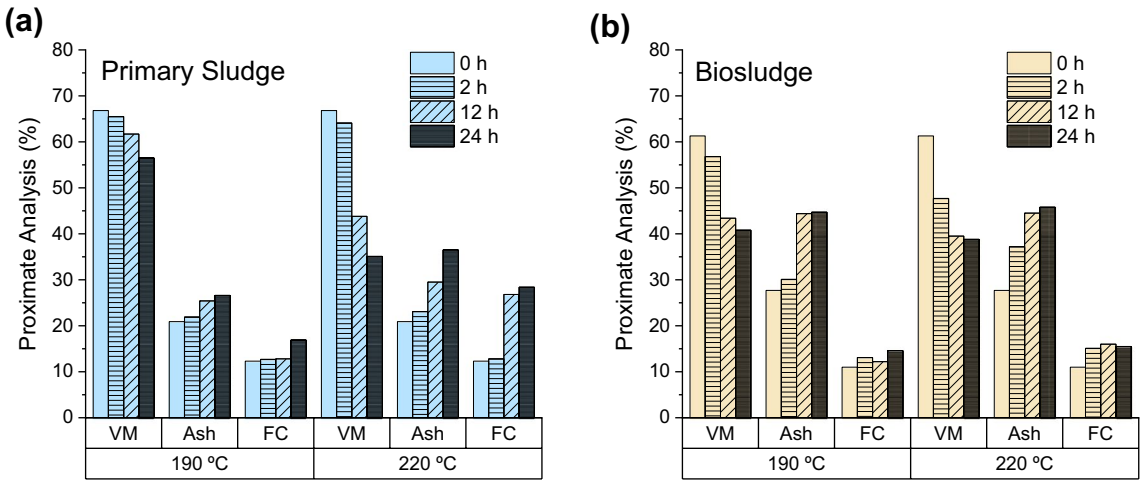

Fig. 2 Evolution of the proximate analysis values on dry basis (Volatile Matter, VM; Ash and; Fixed Carbon, FC) for the hydrochars obtained from: **a** Primary sludge, and **b** Biosludge at different temperatures (190 and 220 ºC), and residence time (2, 12, 24 h). 0 h refers to the untreated feedstock

fixation differently. For instance, hydrochar 220PS24 doubles the content of fixed carbon from 12.3% of the PS to 28.4% (Table S1). In contrast, the volatile matter decreases almost by half, from 66.8% to 35.1%. Conversely, the ash content rises from 20.9% to 36.5%, indicating that practically all the inorganic compounds remain in the solid fraction during the HTC treatment. 220PS24 was selected for further characterization as it shows the highest fixed carbon content. Interestingly, increasing the reaction temperature and residence time does not significantly affect the fixed carbon content for BS as feedstock. For instance, after the hydrothermal treatment at 220 ºC for 2 h (hydrochar 220BS2), it rises from 11 to 15.1%, but it barely changes to 15.5% for 24 h (hydrochar 220BS24). For hydrochar 220BS2, the ash content is 37.2%, considerably higher than that of the untreated BS (27.7%); and the volatile matter content is 47.7% (lower than the value of 61.3% of BS). In terms of energy saving in the process, hydrochar 220BS2 seems more convenient, and it was selected for further characterization.

The scanning electron microscopy (SEM) image enables visual examination of the feedstock morphology before and after the hydrothermal treatment. The SEM image (Fig. 3a) for the primary sludge shows long cellulose fibers that seem to be glued to each other forming skeins without any order. The morphology after the HTC treatment was dramatically altered (Fig. 3b). The fibers lose their identity in the hydrochars 220PS24, and irregular round microparticles appear, similar to flakes. The Energy Dispersive Spectrometry (EDS) measurements show the chemical composition of different zones on the surface particle (Table S2). The results indicate that the carbon content increases from 38.4 to 48.6 wt% while the oxygen content decreases from 55.1 to 39 wt%, which confirms the decomposition of cellulose fibers and the carbon fixation process. Small amounts of inorganic compounds such as Si, Ca, and Al are also detected, most likely coming from the additives and flocculants used in the wastewater treatment plant. In the case of the hydrochar 220BS2, the SEM image resembles as that of BS, except for its larger particle size, indicating that agglutination happens during hydrothermal treatment. In this case, the surface chemical composition of BS and 220BS2 (Table S2) shows very similarly carbon and oxygen content, evidencing the inefficiency in the carbon fixation process. The BS shows Fe, S, P, Mg, and Na apart from Si, Ca, and Al. Na is not detected in the hydrochar 220BS2, indicating that it migrated into the liquid fraction during the hydrothermal process.

The liquid fraction after the HTC process depends on the initial moisture content of the PS and BS and the water/feedstock ratio, which was fixed in *ca* 0.75 and 0.69, respectively. However, hydration water and soluble organic and inorganic compounds from the feedstock are leaching during the hydrothermal process, contributing to the liquid fraction in the mass balance. In addition, organic components of the sludge, such as cellulose, lignin, and hemicellulose, decomposed into smaller products that migrate into the aqueous phase giving a characteristic brownish color. Therefore, physicochemical analysis of the liquid fraction (Table 2) enables further information about the performance of PS and BS feedstock during the hydrothermal process. The resulting values of chemical oxygen demand (COD), total nitrogen (TN), and total phosphorous (TP) are elevated in the liquid fraction of 220BS2 compared to that of 220PS24, being 113 vs. 52.5 g/L DQO, 8900 vs. 42 mg/L TN and 205 vs. 31.5 mg/L TP, respectively. The striking TN value (which includes NH_4^-, NO_3^-, and NO_2^-) can be explained since nitrogen is the nutrient

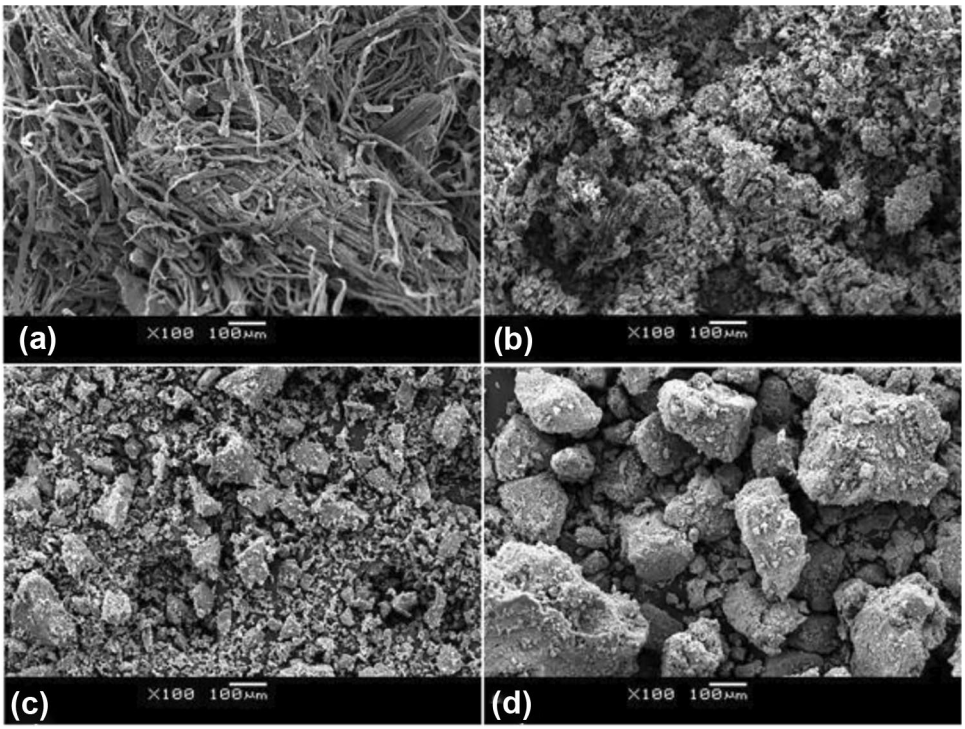

Fig. 3 SEM images for **a** PS, **b** hydrochar 220PS24, **c** BS, **d** hydrochar 220BS2

Table 2 Physic-chemical properties of the liquid fraction for HTC treatment

Feedstock	Temperature °C	Time h	Initial pH	Final pH	COD g/L	TN mg/L	TP mg/L	TSS mg/L
PS	220	24	7	3.9	52.5	42	31.5	1100
BS	220	2	7	7	113	8900	205	380
Decree 253/79 water course				6–9	0.06	5	5	150
Decree 253/79 sewarage				5.5–9.5	0.7*	–	–	700

*BOD value, which is considered as half of COD value, according to reference [32]

(urea) for the active sludge in the reactor, which ends up in the biosluge. Part of it is expected to solubilize in the aqueous phase during the hydrothermal treatment. In addition, nitrogen comes from the deamination of the intensive hydrolysis of proteins, and nucleic acid of the microorganism most likely contributes to the increased TN value [25–27]. The pH 7 remains unchanged after treatment in the case of BS. Conversely, the pH decreases from 7 to 3.9 for PS as feedstock, probably due to the presence of carboxylic acids (i.e., lactic, acetic, formic, propionic acid, among others) produced during the hydrothermal carbonization of the cellulose and other organic compounds such as hemicellulose and lignin [28, 29]. Further investigation of the degradation products in the liquid fraction has to be done to evaluate possible valorization routes [29, 30]. Meanwhile, the water recovery from the HTC treatment must be returned to the wastewater treatment plant before discharge, according to Uruguayan legislation [31].

Fuel Properties

From the ultimate analysis, the elemental composition and the atomic H/C and O/C ratio can be calculated (Table 3). These parameters indicate the degree of biomass condensation and carbon fixation through the decarboxylation (release of CO_2) and dehydration (release of H_2O) reaction [8], which is very well represented in the van Krevelen diagram. It illustrates the successive stages of the geological transformation of the biomass up to reaching anthracite accompanied by energy densification (C–C bond energy is higher than C–O and C–H bonds). According to this diagram, the chemical composition of the PS is located in the biomass area, while the hydrochars 220PS24 approximates to coal (Fig. 4). This is consistent with an increment of the high heat value (HHV) from 12.7 to 17.7 MJ/Kg, which means energy densification of 39%. The fuel ratio (FC/VM) also enhances from 0.18 to 0.81. For BS, the scenario changes, the H and O content decreases, and the fuel ratio increases from 0.18 to 0.31. However, a diminution in the carbon content prevents

Table 3 Fuel properties for PS and BS feedstocks, and hydrochars 220PS24 and 220BS2

		PS	220PS24	BS	220BS2
Ultimate analysis (wt%)	C	35.21	45.1	36.88	35.70
	H	5.04	4.10	5.79	4.80
	N	0.42	0.80	5.34	3.90
	S	0.15	0.10	1.15	0.70
	O	38.28	13.40	23.10	17.70
Atomic Ratio	H/C	1.72	1.09	1.88	1.61
	O/C	0.81	0.22	0.47	0.37
	N/C	0.01	0.02	0.12	0.09
High heat value (MJ/kg)		12.7	17.7	16.0	15.4
Energy densification[1]		–	1.39	–	0.96
Energy conversion efficiency of the process (%)[2]			57		48
Fuel ratio[3]		0.18	0.81	0.18	0.31

[1]Energy densification = HHV of hydrochar/HHV of feedstock

[2]Energy conversion efficiency of the process = (HHV of hydrochar/HHV of feedstock) solid yield

[3]Fuel ratio = fixed carbon/volatile matter

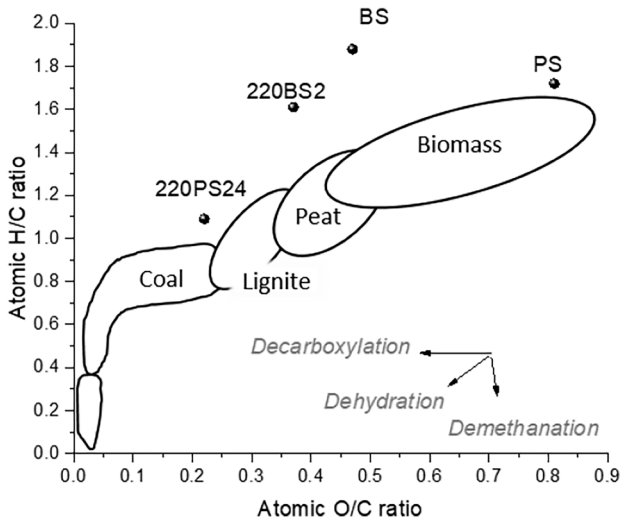

Fig. 4 Van Krevelen diagram for PS and BS feedstocks, and hydrochars 220PS24 and 220BS2

the energy densification of this kind of biomass waste. The HHV is practically identical for BS and 220BS2, being 16 and 15.4 MJ/Kg, respectively. The position in the van Krevelen diagram of 220BS2 is similar to that of peat. Last but not least, the energy conversion efficiency of the process calculated according to ref [33] is 57% and 48% for PS and BS feestocks. This value takes into account not only the high heat value but also the carbon yield.

Despite the lack of energy densification for BS after hydrothermal treatment, its fuel quality can still enhance. For instance, a low sulfur (S) and nitrogen (N) content in fuel is desirable because the production of SOx and NOx emissions during the combustion would diminish. In this sense, the hydrothermal treatment reduced the S content in both feesdstocks (Table 3). The nitrogen content is very small in the case of PS (0.42%) and decreases from 5.34 to 3.9% in BS, indicating that a deamination reaction is taking place. Indeed, the TN in the liquid fraction was very high (Table 2). It is worth to mention, that the nitrogen seems to be retained in the hydrochar 220PS24 (from 0.42 to 0.80%). Lilian et al. reported that a high temperature promotes the deamination of biomass-containing protein, enriching the liquid fraction during the HTC treatment, as in BS. However, when lignocellulosic biomass is in the reaction medium, the Millard and Mannich reactions promote the retention of the N in the hydrochar [25]. This phenomenon is crucial for some applications where the nitrogen functional group in hydrochar gains relevance [27, 34], such as for CO_2 capture applications [34] or supercapacitor applications [35].

Thermogravimetric analysis (TG) in air and its derivative (DTG) is used to determine the combustion characteristics of PS, BS, and the hydrochars 220PS24 and 220BS2 (Fig. 5). The TG curves usually show a minor first weight decay below 100 ºC corresponding to moisture. After this dehydration, the decomposition of volatile matter commences, followed by oxidation [36]. In the case of an oxidative atmosphere, combustion and devolatilization might happen simultaneously. The TG curves obtained for PS show a weight decay with a maximum in DTG at 320 ℃, which is generally assigned to cellulose decomposition [37], and a small peak at 416 ℃, which is attributed to lignin decomposition. For hydrochar 220PS24 the combustion profile is altered. A single weight loss exhibiting a maximum in DTG at 425 ℃, and a shoulder at 320 ℃ indicates that the cellulose almost completely decomposes during the hydrothermal process to form a more stable organic compound. The TG curves for BS show two well-marked weight decays. The first one is attributed to the decomposition of the volatile matter, and has its maximum rate of decay at 272 ℃. The second one is sharper and exhibits a peak in DTG at 505 ℃, indicating the combustion of fixed carbon. After hydrothermal treatment, hydrochar 220BS2 exhibits a single peak in DTG at 300 ℃ accompanied by a shoulder a higher temperature, indicating the decomposition of less reactive biomass. Complementary TGs in an inert atmosphere for PS and BS were performed (Fig. S2). Profiles show a prominent weight decay with a maximum in DTG at 350 ºC and 300 ºC, for PS and BS, respectively, which confirms the decomposition of volatile matter of these feedstocks at these temperatures.

Combustion temperature and combustibility index obtained from the TG and DTG curves allows for a quantitative comparison between the feedstocks and their corresponding hydrochars. They are summarized in Table 4. The ignition temperature (T_i) represents the temperature at which

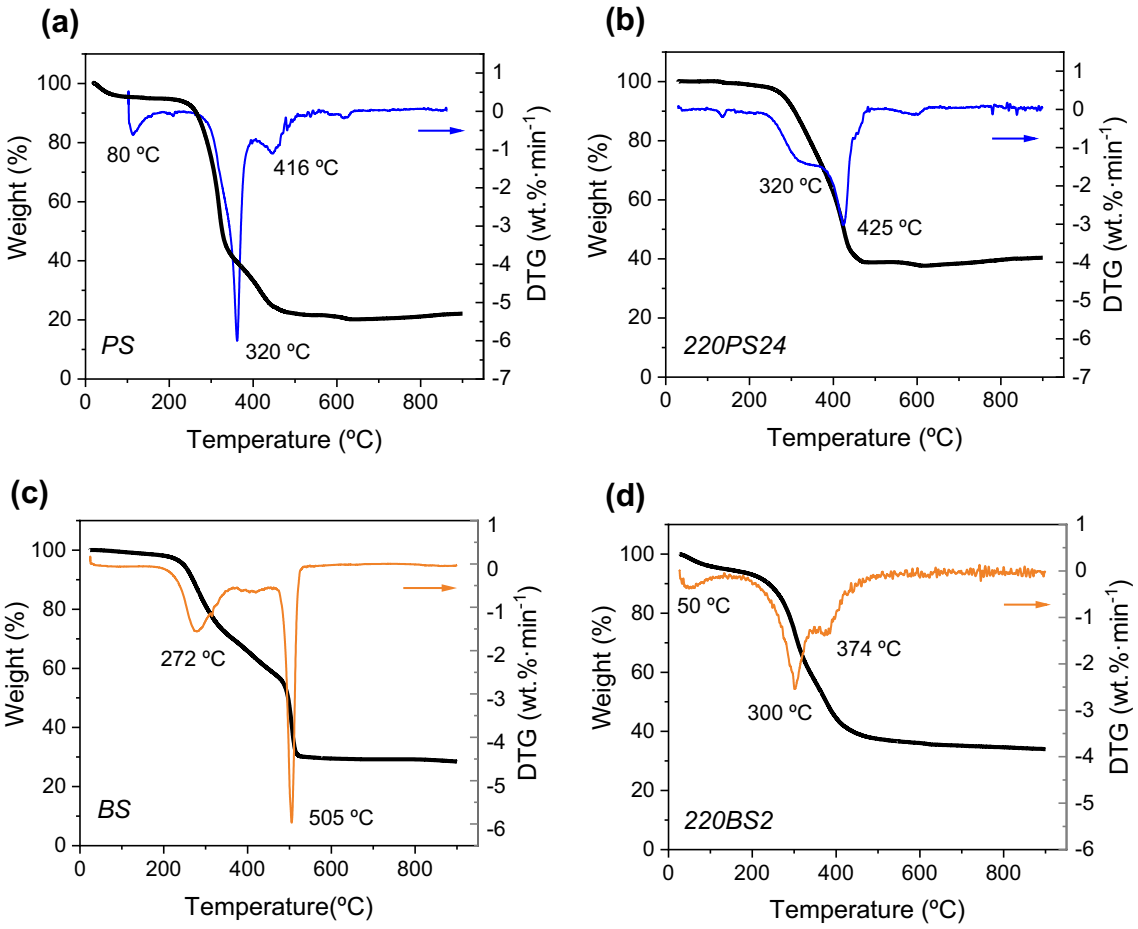

Fig. 5 TG and DTG curves for **a** Primary sludge (PS), **b** hydrochar 220PS24, **c** Biosludge (BS), and **d** hydrochar 220BS2. Heating rate of 5 °C/min in air flow of 50 ml/min

Table 4 Combustion parameters of the primary sludge and biosludge compared to their corresponding hydrochars (heating rate: 5 °C/min)

	PS	220PS24	BS	220BS2
Ignition temperature, T_i (°C)	266	294	256	262
Ignition time, t_i (min)	50.27	53.57	47.3	47.93
Burnout temperature, T_b (°C)	531	490	534	532
Burnout time, t_b (min)	103.17	92.63	102.67	101.67
Maximum peak temperature, T_p (°C)	320	425	272	305
Maximum peak time, t_p (min)	61	79.63	51.83	56.37
Maximum combustion rate, DTG_{max} (wt%/min)	6	3	1.56	2.54
Mean combustion rate, DTG_{mean} (wt%/min)	1.54	0.76	0.6	0.58
Time range of DTG/DTG $_{max}$ = 0.5, $t_{0.5}$ (min)	56.5	68.53	45.83	50
[1]Ignition index, D_i (wt%/min^3 ·10^{-3})	2.0	0.7	0.6	0.9
[2]Burnout index, D_b (wt%/min^3 ·10^{-3})	1.7	0.6	0.6	0.9
[3]Combustion index, S (wt%^{2}/(min^2 ·°C^3)·10^{-8})	24.6	5.4	2.7	4.0
[4]Combustion stability index, H_f (°C·10^3)	1.2	1.9	1.2	1.4

[1]$D_i = DTG_{max}/(t_p \cdot t_i)$; [2]$D_b = DTG_{max}/(t_{0.5} \cdot t_p \cdot t_b)$; [3]$S = DTG_{max} \cdot DTG_{mean}/(T_i^2 \cdot T_b)$; [4]$H_f = T_p \cdot \ln(t_{0.5}/DTG_{mean})$

Table 5 Inorganic content of ashes from the combustion of primary sludge (PS), biosludge (BS), hydrochar 220PS24 and hydrochar 220BS2 by XRF in wt%

	PS ash	220PS24 ash	BS ash	220BS2 ash
Normalized percentage of stable Oxide (% wt)				
SiO_2	41.96	45.03	30.19	30.05
CaO	29.10	20.93	15 .89	17.05
Al_2O_3	10.10	11.43	12.19	14.26
SO_3	8.63	6.45	17.09	11.79
Fe_2O_3	5.14	7.71	8.05	9.97
TiO_2	1.96	2.90	0.78	0.65
K_2O	1.93	1.51	1.91	0.89
P_2O_5	0.74	1.71	9.17	9.41
MgO	0.00	1.73	3.24	4.02
MnO	0.44	0.60	1.50	1.92
Slagging and fouling indexes				
B ($+P_2O_5$)	36.91	33.59	38.26	41.34
A	54.02	59.36	43.16	44.96
$R_{B/A}$	0.68	0.57	0.89	0.92
R_S	0.10	0.06	1.02	0.64
F_u	1.32	0.85	1.69	0.83

Table 6 Textural properties and CO_2 adsorption performance of PS-AC, BS-AC, 220PS2-AC and 220BS2-AC

	PS -AC	220PS24 - AC	BS -AC	220BS2 -AC
Textural properties				
SSA_{BET} (m^2/g)	800	683	120	58
$V_{t,0.9}$ (cm^3/g)	0.63	0.39	0.10	0.09
$V_{N2,DR}$ (cm^3/g)	0.26	0.23	0.04	0.02
$V_{CO2,DR}$ (cm^3/g)	0.25	0.20	0.02	0.04
V_{meso} (cm^3/g)	0.37	0.16	0.06	0.07
Ash (wt%)	38.6	45.8	63.6	53.5
CO_2 adsorption capacity (mmol/g)				
1 bar/10 bar, 273 K	1.30/5.00	1.35/4.35	0.21/0.38	0.48/0.92
1 bar/10 bar, 298 K	0.77/3.26	0.81/2.86	0.15/0.34	0.33/0.73
1 bar/10 bar, 323 K	0.46/2.33	0.50/2.13	0.07/0.29	0.20/0.60

the sample starts to burn. Results indicate that the hydrothermal carbonization raises the maximum peak temperature (T_p) in DTG and slightly delays the ignition time for both feedstocks. The hydrothermal treatment considerably lowers the values of the ignition (D_i), burnout (D_b), and combustion (S) indexes for PS, which means that the untreated PS is easier to ignite, and its combustion activity is higher than 220PS24. The result is expected since PS contains more volatile matter than the hydrochar, consequently it ignites in a more violent reaction. For BS, combustibility indexes are slightly enhanced after the hydrothermal treatment. Note that BS exhibits two DTG peaks; the first one (lower temperature) was used for this evaluation. Nonetheless, a higher combustion stability index (H_f) for both 220PS24 and 220BS2 indicates a more stable fuel than untreated feedstocks [17].

Due to a large ash content in PS (20.9 wt%) and BS (27.7 wt%) and that this amount considerably rises in 220PS24 (36.5 wt%) and 220BS2 (37.2 wt%), it is worth analyzing how the ash chemical constitution changes after the HTC treatment (Table 5). It has been found that basic compounds decrease the melting temperature of ashes, promoting severe slagging and fouling process, while acidic compounds increase it conversely [38]. Therefore, the basic to acid oxide ratio ($R_{B/A}$) can predict the slagging and fouling tendency in an industrial fluidized bed biomass boiler [18, 39], see Eq. 6–8. Originally, the $R_{B/A}$ ratio was introduced for fossil fuels with low phosphorous content. Pronobis suggested in ref [19] to incorporate P_2O_5 since it contributes to developing low-melting-point phases in ash. In the particular case of BS, a large anomaly amount of phosphorus is found due to the special composition of the Eucalyptus used in the pulp plant in Uruguay. Results reveal that the hydrothermal treatment diminishes the $R_{B/A}$ value for PS but slightly increases for BS (Table 5). Nonetheless, the slagging index (R_S) decreases after the hydrothermal treatment for both feedstocks because the sulfur content is considerably reduced. Whereas for 220PS24, R_S is as low as 0.06, and for 220BS24 is 0.64. A R_S value lower than 0.6 implies low slagging inclination [19, 39, 40]. Regarding the fouling index (F_u), the results are also promising. F_u value diminishes almost by half in both PS and BS cases, from 1.32 to 0.85 and 1.69 to 0.83, respectively. This is from a strong ($0.6 < F_u < 40$) toward low tendency to form deposits ($F_u \leq 0.6$) [39], confirming HTC is an effective method to diminish the fouling tendency thanks to the water solubility nature of K and Na (main responsible for fouling) that leach during the hydrothermal treatment. Similar behavior was reported by Lin et al. [41]. Summarizing, the HTC treatment enhances the fuel quality (less N and S content), produces a more stable biofuel (lower H_f), and mitigates the risk of slagging and fouling.

Valorization via Activated Carbon Production

PS, BS, and their hydrochars 220PS24 and 220BS2 are cheap precursors to produce valuable activated carbons (ACs). SEM images in Fig. S8 show particles with amorphous structures in all cases, with no significant differences between them. Table 6 reports the textural characteristics of the ACs prepared by chemical activation of sluges

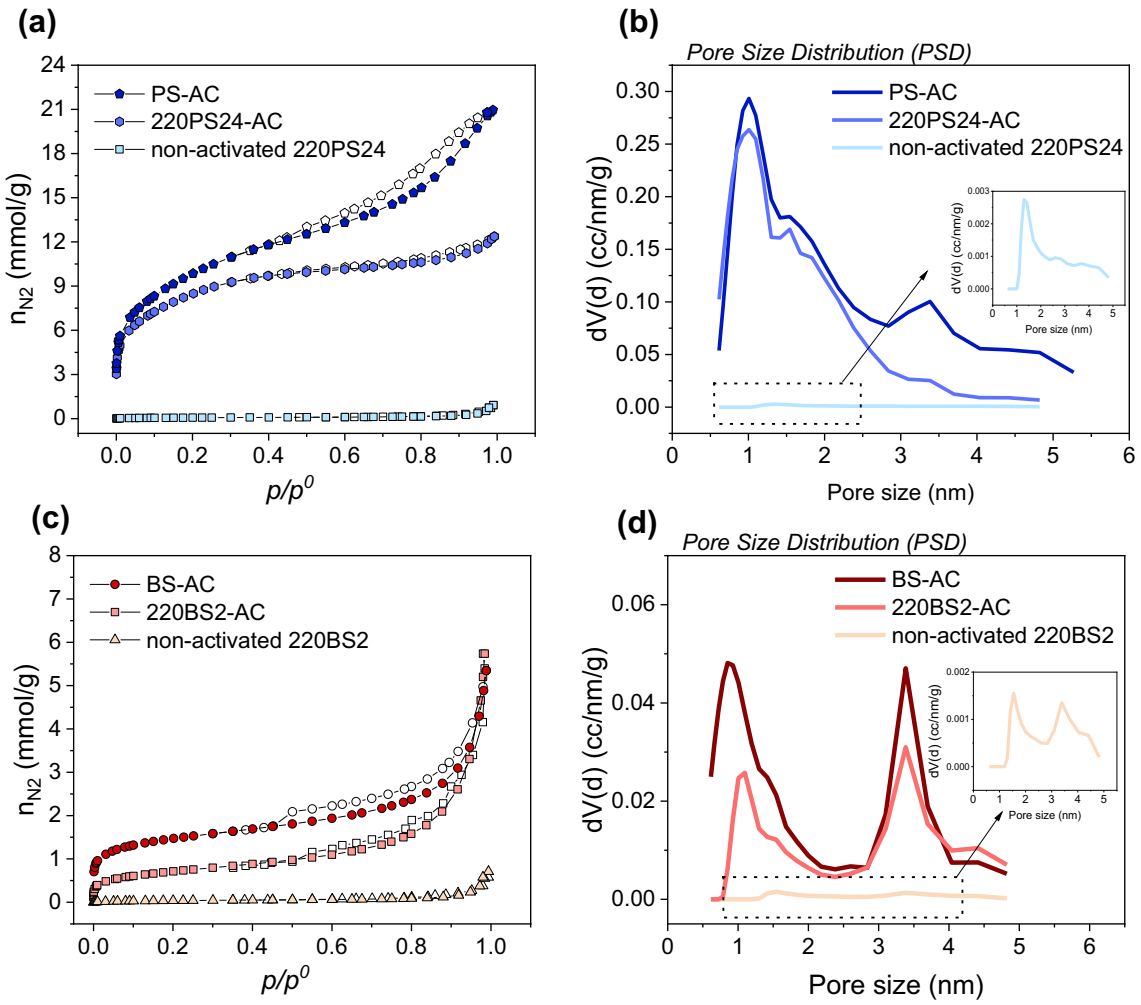

Fig. 6 Nitrogen adsorption (full point)/desorption (empty point) isotherms at 77 K for activated carbon using as feedstocks: **a** primary sludge, **c** biosludge. Pore size distribution (PSD) obtained for activated carbon using as feedstocks: **b** primary sludge, **d** biosluge

and hydrochars with phosphoric acid, including the BET specific surface area (SSA_{BET}), total pore volume ($V_{t,0.9}$), microporosity calculated by DR equation to the nitrogen and carbon dioxide isotherms ($V_{N2,DR}$ and $V_{CO2,DR}$) and mesopore volume (V_{meso}). The specific surface area for PS-AC and 220PS24-AC are very promising, considering the extremely high ash content in these samples (SSA_{BET} = 800 and 683 m^2/g, respectively). The reported values are comparable to those of commercial massive activated carbons imported and used in different industrial processes in Uruguay to eliminate pollutants, discoloration, and wastewater treatment plants, among others applications (Fig. S4, Table S3). Furthermore, there is room to enhance the quality of the activated carbons obtained in this work. For instance, acid and base post-treatment methods can be improved the textural properties through the elimination of the inorganic compounds from the carbonaceous matrix [42]. If so, the SSA_{BET} of PS-AC expressed on free-ash basis is as high as 1300 m^2/g. Conversely, BS and 220BS2 produces activated carbons with lower surface area (SSA_{BET} = 120 and 58 m^2/g, respectively). Besides, this strategy is smart to immobilize heavy metal coming from sludges.

The nitrogen adsorption/desorption isotherm of 220PS24-AC shows a type I(b) curve at low relative pressure and a type IV(a) with hysteresis loop type H4, according to the IUPAC classification (Fig. 6). This kind of isotherm is found with materials having pore size distribution over a broader range, including wider micropores (< 2 nm) and narrow mesopores (< ~ 2.5 nm) [43]. Isotherm of PS-AC shows a similar shape (maximum in PSD at 1.1 nm), although a hysteresis loop indicates the presence of mesopores that can be seen in the PSD curve with a maximum at 3.5 nm pore size. For BS-AC and 220BS2-AC, the scenario completely changes. Isotherms are type I(b) + IV(a). Type IV(a) curve is given for samples showing pores condensation in mesopores [43]. A bimodal pore size distribution (PSDs)

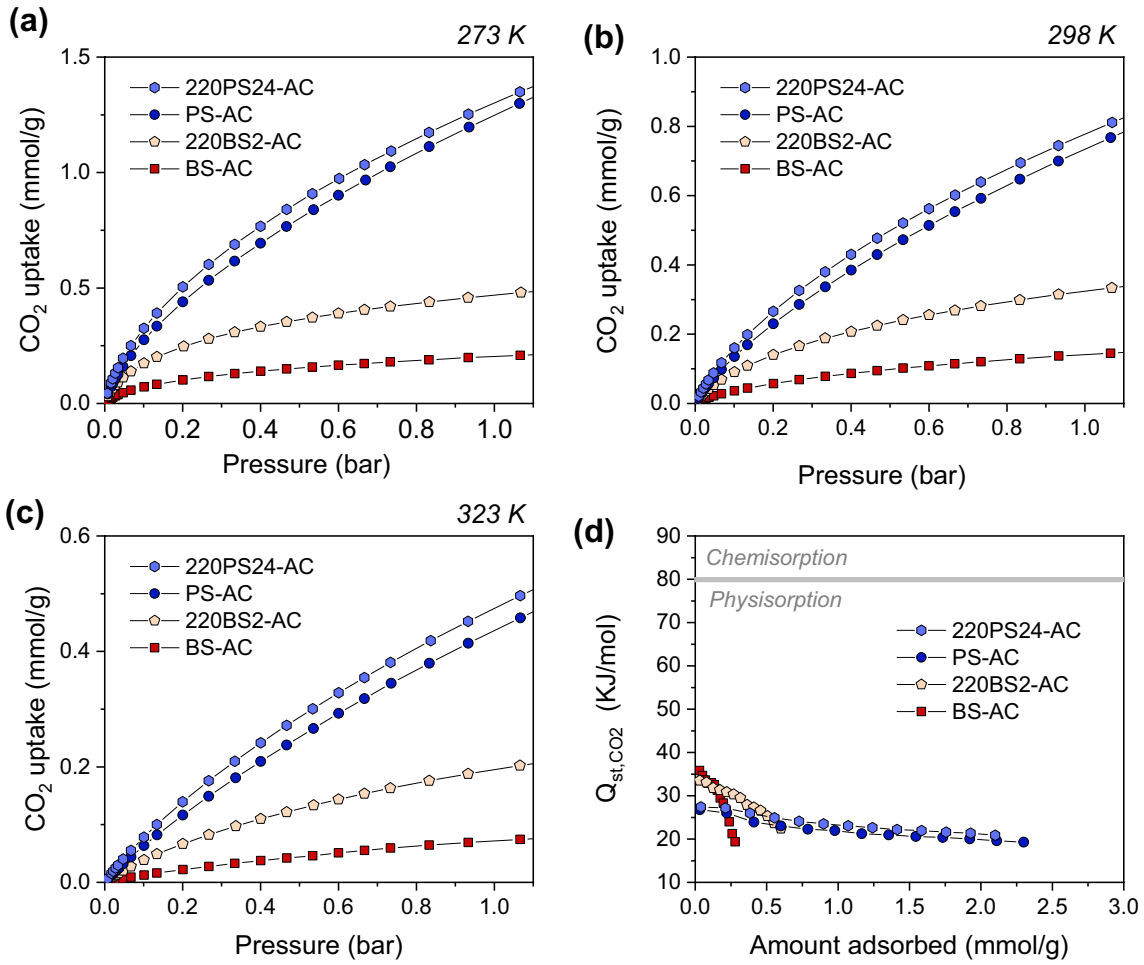

Fig. 7 CO_2 adsorption isotherms for the activated carbons PS-AC, 220PS24-AC, BS-AC and 220BS2-AC at three temperatures: **a** 273 K, **b** 298 K, and **c** 323 K; and **d** Isosteric heat of CO_2 adsorption ($Q_{st,CO2}$)

curve confirms this classification since two maxima in the micropores and narrow mesoporous regions can be seen, i.e. at 1 nm and at 3.5 nm, respectively. The non-activated hydrochars isotherms are typical of nonporous or macropores adsorbents (type II). Doing a zoom on this curve (Fig. S5), the shape results from the monolayer coverage completion by the adsorbate, point B, with low specific surface areas. Hydrochar 220PS24 exhibits a SSA_{BET} equal to 3.3 m^2/g while hydrochar 220BS2, 5.5 m^2/g.

CO_2 adsorption isotherms at 273 K allow for a more accurate characterization in the ultra- microporous range (< 1 nm) [44]. Interestingly, the pores size distribution in Fig. S6 confirms a displacement of the maximum toward a smaller pore size when the raw material is hydrothermally treated. A more ordered and uniform structure obtained by the HTC method gives rise to a more microporous activated carbon using the same activation condition (i.e., amount of phosphoric acid, temperature, and activation time). This phenomenon is critical when designing an activated carbon for a specific application. The obtained activated carbon will be tested for CO_2 capture in the following section.

CO_2 Adsorption Performance

The CO_2 adsorption capacity was measured at three temperatures, 273, 298, and 323 K, up to 10 bar (Fig. S7). 220PS24-AC shows a value of 1.35 mmol/g at 273 K at 1 bar, followed by PS-AC, which adsorbs 1.30 mmol/g. A narrower pore size distribution of the activated hydrochar explains its best performance at low pressure (Fig. 7). However, the trend changes at higher pressure, i.e., 10 bar. PS-AC uptakes an amount as high as 5 mmol/g, while 220PS24-AC uptakes 4.35 mmol/g, evidencing that at higher pressure, narrow mesoporous plays a role in adsorbing CO_2 [45]. The best performance is found for 220BS2-AC compared to BS-AC in the studied pressure range. The presence of ultramicropores in 220BS2-AC might explains these results. Indeed, Fig. S6, compares the micropore size distribution

of samples calculated by applying the Horwath-Kawazoe method for pore with slit geometries to the CO_2 adsorption data at 273 K. This analysis complements that obtained by applying the QSDFT method to the N_2 adsorption data at 77 K since the entry of nitrogen to ultramicropores (< 1 nm) is restricted at 77 K. Sample 220BS2-AC shows a narrower distribution with a maximum shifted to lower pore size (*ca.* 0.6 nm), where a higher CO_2 adsorption potential is expected [45].

The higher adsorption capacity was observed at the lowest temperature (Table 6) due to the exothermic nature of the adsorption phenomenon. In this sense, the heat of adsorption was calculated for the four samples. A value between 25 and 35 kJ/mol indicates that physisorption is taking place. Furthermore, for PS-AC and 220PS24-AC, the heat of adsorption remains almost constant (around 25–20 kJ/mol), with the coverage degree indicating homogeneity in the active sites (Fig. 7c). On the other hands, BS-AC and 220BS2-AC present highly energetic sites, around 35 kJ/mol. Nonetheless, this interaction decreases with the degree of coverage. This observation concurs with the presence of ultramicropores with high adsorption potential, although the influence of nitrogen functional groups in the adsorbent surface increasing the adsorbate-adsorbent interaction cannot be ruled out (See XPS results in Figs. S9–S11 and Table S4). The CO_2 uptake values reported here are similar to those found in the literature, despite the ash contain, which contributes to the weight but is not active in adsorbing CO_2. Although BS and PS are a problem for the industry, we demonstrated that they could be transformed into valuable products to capture a critical greenhouse gas.

Conclusion

Herein, we demonstrated that the hydrothermal carbonization technique enhances the combustion performance of PS and BS, for instance, a higher combustion stability index (H_f) for both 220PS24 and 220BS2 indicates a more stable fuel than untreated feedstocks. The HTC had a better effect on PS than BS in energy densification (1.39 vs. 0.96 respectively). Nonetheless, for BS, the removal of 40% of sulfur and 28% of nitrogen is advantageous in order to release less amount of NOx and SOx during incineration. HTC is also attractive to diminish the slagging (0.1 to 0.06 for PS and 1.02 to 0.64 for BS) and fouling (0.32 to 0.85 for PS and 1.69 to 0.83 for BS) indexes increasing the life expectancy of boilers. As an alternative to incineration, we proposed using BS and PS and their hydrochars as precursors to synthesize activated carbons able to adsorb CO_2 (i.e. the BET specific surface area was as high as 800 m^2/g for PS-AC, and exhibits CO_2 adsorption capacity of 5 mmol/g at 10 bar at 273 K). Apart from producing valuable products to face air pollution, this option is an effective strategy to immobilize heavy metals from sludges.

Supplementary Information The online version contains supplementary material available at https://doi.org/10.1007/s12649-023-02105-8.

Acknowledgements MEC acknowledges Cristian Toncón for the nitrogen sorption measurements, Dimar Villarroel Rocha for carbon dioxide sorption measurements, Mauricio Ohanian for XRF measurements, Gastón Cubas for providing the residues used as feedstocks. MEC acknowledges the Alexander von Humboldt foundation for the Return Fellowship.

Author Contributions MEC and MD contributed to the study conception and design. Material preparation was performed by VM. Data collection and analysis were performed by MEC, KS and AC. The first draft of the manuscript was written by MEC and all authors commented on previous versions of the manuscript. All authors read and approved the final manuscript.

Funding The Agencia Nacional de Investigación e Innovación for financial support (PD_NAC_2018_1_150145).

Data Availability Not applicable.

Code Availability Not applicable.

Declarations

Conflict of interest The authors have no conflicts of interest to declare that are relevant to the content of this article.

References

1. Planta de celulosa con tecnología de vanguardia. https://www.upmpasodelostoros.com/es/planta-de-celulosa/. Accessed 14 Mar 2023
2. Montes del Plata. Producción sustentable. https://www.montesdelplata.com.uy/espanol/. Accessed 14 Mar 2023
3. C. Amorin. https://www.ambiente.gub.uy/oan/wp-content/uploads/2018/02/VAL_Planta-de-celulosa-Paso-de-los-Toros-.pdf. Accessed 1 Nov 2022
4. Bentancur, S., López-Vázquez, C.M., García, H.A., Duarte, M., Travers, D., Brdjanovic, D.: Modelling of a pulp mill wastewater treatment plant for improving its performance on phosphorus removal. Process Saf. Environ. Prot. **146**, 208–219 (2021). https://doi.org/10.1016/j.psep.2020.08.029
5. Mohammadi, A., Sandberg, M., Venkatesh, G., Eskandari, S., Dalgaard, T., Joseph, S., Granström, K.: Environmental analysis of producing biochar and energy recovery from pulp and paper mill biosludge. J. Ind. Ecol. **23**(5), 1039–1051 (2019). https://doi.org/10.1111/jiec.12838
6. Martínez, J., Mallo, M., Lucas, R., Álvarez, J., Salvarrey, A., Gristo, P. Guía para la gestión integral de residuos peligrosos. Fundamentos. Tomo I. (2005) https://www.cempre.org.uy/docs/biblioteca/guia_para_la_gestion_integral_residuos/gestion_respel01_fundamentos.pdf. Accessed 1 Nov 2022
7. Sevilla, M., Fuertes, A.B.: Chemical and structural properties of carbonaceous products obtained by hydrothermal carbonization of saccharides. Chem. Eur. J. **15**(16), 4195–4203 (2009). https://doi.org/10.1002/chem.200802097
8. Libra, J.A., Kyoung, S.R., Kammann, C., Funke, A., Berge, N.D., Neubauer, Y., Titirici, M.M., Fühner, C., Bens, O., Kern,

J., Emmerich, K.H.: Hydrothermal carbonization of biomass residuals: a comparative review of the chemistry, processes and applications of wet and dry pyrolysis. Biofuels **2**(1), 71–106 (2014). https://doi.org/10.4155/bfs.10.81
9. Jain, A., Balasubramanian, R., Srinivasan, M.P.: Hydrothermal conversion of biomass waste to activated carbon with high porosity: A review. Chem. Eng. J. **283**, 789–805 (2016). https://doi.org/10.1016/j.cej.2015.08.014
10. Ischia, G., Fiori, L.: Hydrothermal carbonization of organic waste and biomass: A review on process, reactor, and plant modeling. Waste Biomass Valoriz. **12**, 2797–2824 (2021). https://doi.org/10.1007/s12649-020-01255-3
11. Hu, B., Wang, K., Wu, L., Yu, S.H., Antonietti, M., Titirici, M.M.: Engineering carbon materials from the hydrothermal carbonization process of biomass. Adv. Mater. **22**(7), 813–828 (2010). https://doi.org/10.1002/adma.200902812
12. Lu, X., Berge, N.D.: Influence of feedstock chemical composition on product formation and characteristics derived from the hydrothermal carbonization of mixed feedstocks. Bioresour. Technol. **166**, 120–131 (2014). https://doi.org/10.1016/j.biortech.2014.05.015
13. Saha, N., Saba, A., Saha, P., McGaughy, K., Franqui-Villanueva, D., Ortz, W.J., Hart-Cooper, W., Reza, T.M.: Hydrothermal carbonization of various paper mill sludges: An observation of solid fuel properties. Energies **12**(5), 858 (2019). https://doi.org/10.3390/en12050858
14. Monte, M.C., Fuente, E., Blanco, A., Negro, C.: Waste management from pulp and paper production in the European Union. Waste Manag. **29**(1), 293–308 (2009). https://doi.org/10.1016/j.wasman.2008.02.002
15. Wilk, M., Śliz, M., Lubieniecki, B.: Hydrothermal co-carbonization of sewage sludge and fuel additives: Combustion performance of hydrochar. Renew. Energy **178**, 1046–1056 (2021). https://doi.org/10.1016/j.renene.2021.06.101
16. Mureddu, M., Dessì, F., Orsini, A., Ferrara, F., Pettinau, A.: Air- and oxygen-blown characterization of coal and biomass by thermogravimetric analysis. Fuel **212**, 626–637 (2018). https://doi.org/10.1016/j.fuel.2017.10.005
17. Zhang, Y., Guo, Y., Cheng, F., Yan, K., Cao, Y.: Investigation of combustion characteristics and kinetics of coal gangue with different feedstock properties by thermogravimetric analysis. Thermochim. Acta **614**, 137–148 (2015). https://doi.org/10.1016/j.tca.2015.06.018
18. Yang, S., Lei, M., Li, M., Liu, C., Xue, B., Xiao, R.: Comprehensive estimation of combustion behavior and thermochemical structure evolution of four typical industrial polymeric wastes. Energies **15**(7), 2487 (2022). https://doi.org/10.3390/en15072487
19. Pronobis, M.: Evaluation of the influence of biomass co-combustion on boiler furnace slagging by means of fusibility correlations. Biomass Bioenerg. **28**(4), 375–383 (2005). https://doi.org/10.1016/j.biombioe.2004.11.003
20. Rouquerol, J., Llewellyn, P., Rouquerol, F.: Is the bet equation applicable to microporous adsorbents. Stud. Surf. Sci. Catal. **160**, 49–56 (2007). https://doi.org/10.1016/s0167-2991(07)80008-5
21. Ruthven, D.M.: Principles of adsorption and adsorption processes. Wiley, New York (1984)
22. Faroppa, C., Annala, K.: Informe Ambiental. Resumen. Expediente 2004/14001/1/01177. Botnia. 2004. http://www.guayubira.org.uy/celulosa/EIA-Botnia.pdf. Accessed 1 Nov 2022
23. Inoue, S., Sawayama, S., Dote, Y., Ogi, T.: Behaviour of nitrogen during liquefaction of dewatered sewage sludge. Biomass Bioenergy **12**(6), 473–475 (1997). https://doi.org/10.1016/S0961-9534(97)00017-2
24. He, C., Giannis, A., Wang, J.Y.: Conversion of sewage sludge to clean solid fuel using hydrothermal carbonization: Hydrochar fuel characteristics and combustion behavior. Appl. Energy **111**, 257–266 (2013). https://doi.org/10.1016/j.apenergy.2013.04.084
25. Leng, L., Yang, L., Leng, S., Zhang, W., Zhou, Y., Peng, H., Li, H., Hu, Y., Jiang, S., Li, H.: A review on nitrogen transformation in hydrochar during hydrothermal carbonization of biomass containing nitrogen. Sci. Total Environ. **756**, 143679 (2021). https://doi.org/10.1016/j.scitotenv.2020.143679
26. Zhuang, X., Huang, Y., Song, Y., Zhan, Y., Yin, X., Wu, C.: The transformation pathways of nitrogen in sewage sludge during hydrothermal treatment. Bioresour. Technol. **245**, 463–470 (2017). https://doi.org/10.1016/j.biortech.2017.08.195
27. Xu, Z.-X., Ma, X.-Q., Zhou, J., Duan, P.-G., Zhou, W.-Y., Ahmad, A., Luque, R.: The influence of key reactions during hydrothermal carbonization of sewage sludge on aqueous phase properties: A review. J. Anal. Appl. Pyrol. **167**, 105678–105701 (2022). https://doi.org/10.1016/j.jaap.2022.105678
28. Weiner, B., Poerschmann, J., Wedwitschka, H., Koehler, R., Kopinke, F.D.: Influence of process water reuse on the hydrothermal carbonization of paper. ACS Sustain. Chem. Eng. **2**(9), 2165–2171 (2014). https://doi.org/10.1021/sc500348v
29. Xiao, L.P., Shi, Z.-J., Xu, F., Sun, R.-C.: Hydrothermal carbonization of lignocellulosic biomass. Bioresour. Technol. **118**, 619–623 (2012). https://doi.org/10.1016/j.biortech.2012.05.060
30. Langone, M., Basso, D.: Process waters from hydrothermal carbonization of sludge: characteristics and possible valorization pathways. Int. J. Environ. Res. Public Health **17**(18), 6618 (2020). https://doi.org/10.3390/ijerph17186618
31. Decreto N 253/979. https://www.impo.com.uy/bases/decretos/253-1979. Accessed 1 Nov 2022
32. Aziz, J.A., Tebbutt, T.H.Y.: Significance of COD, BOD and TOC correlations in kinetic models of biological oxidation. Water Res. **14**(4), 319–324 (1980). https://doi.org/10.1016/0043-1354(80)90077-9
33. Antal, M.J., Grønli, M.: The art, science, and technology of charcoal production. Ind. Eng. Chem. Res. **42**(8), 1619–1640 (2003). https://doi.org/10.1021/ie0207919
34. Canevesi, R.L.S., Schaefer, S., Izquierdo, M.T., Celzard, A., Fierro, V.: Roles of surface chemistry and texture of nanoporous activated carbons in CO2 capture. ACS Appl. Nano Mater. **5**(3), 3843–3854 (2022). https://doi.org/10.1021/acsanm.1c04474
35. Xu, Z.-X., Deng, X.-Q., Zhang, S., Shen, Y.-F., Shan, Y.-Q., Zhang, Z.-M., Luque, R., Duan, P.-G., Hu, X.: Benign-by-design N-doped carbonaceous materials obtained from the hydrothermal carbonization of sewage sludge for supercapacitor applications. Green Chem. **22**(12), 3885–3895 (2020). https://doi.org/10.1039/D0GC01272F
36. Biagini, E., Tognotti, L.: Comparison of devolatilization/char oxidation and direct oxidation of solid fuels at low heating rate. Energy Fuels **20**(3), 986–992 (2006). https://doi.org/10.1021/ef0503156
37. Yang, H., Yan, R., Chen, H., Zheng, C., Lee, D.H., Liang, D.T.: In-depth investigation of biomass pyrolysis based on three major components: hemicellulose, cellulose and lignin. Energy Fuels **20**(1), 388–393 (2006). https://doi.org/10.1021/ef0580117
38. Song, W.J., Tang, L.H., Zhu, X.D., Wu, Y.Q., Zhu, Z.B., Koyama, S.: Effect of coal ash composition on ash fusion temperatures. Energy Fuels **24**(1), 182–189 (2009). https://doi.org/10.1021/ef900537m
39. Pronobis, M., Kalisz, S., Polok, M.: The impact of coal characteristics on the fouling of stoker-fired boiler convection surfaces. Fuel **112**, 473–482 (2013). https://doi.org/10.1016/j.fuel.2013.05.044
40. Miles, T.R., Miles, T.R.J., Baxter, L.L., Bryers, R.W., Jenkins, B.M., Oden, L.L.: Boiler deposits from firing biomass fuels. Biomass Bioenergy **10**(2–3), 125–138 (1996). https://doi.org/10.1016/0961-9534(95)00067-4

41. Lin, Y., Ma, X., Peng, X., Hu, S., Yu, Z., Fang, S.: Effect of hydrothermal carbonization temperature on combustion behavior of hydrochar fuel from paper sludge. Appl. Therm. Eng. **91**, 574–582 (2015). https://doi.org/10.1016/j.applthermaleng.2015.08.064
42. Aliakbari, Z., Younesi, H., Ghoreyshi, A.A., Bahramifar, N., Heidari, A.: Production and characterization of sewage-sludge based activated carbons under different post-activation conditions. Waste Biomass Valoriz. **9**(3), 451–463 (2018). https://doi.org/10.1007/s12649-016-9823-7
43. Thommes, M., Kaneko, K., Neimark, A., Olivier, J.P., Rodríguez-Reinoso, F., Rouquerol, J., Sing, K.S.W.: Physisorption of gases, with special reference to the evaluation of surface area and pore size distribution (IUPAC Technical Report). Pure Appl. Chem. **87**(9–10), 1051–1069 (2015). https://doi.org/10.1515/pac-2014-1117
44. Garrido, J., Linares-solano, A., Martín-Martínez, M., Rodríguez-Reinoso, F., Torregrosa, R.: Use of nitrogen vs carbon dioxide in the characterization of activated carbons. Langmuir **3**(1), 76–81 (1987). https://doi.org/10.1021/la00073a013
45. Casco, M.E., Martínez-Escandell, M., Silvestre-Albero, J., Rodrígue-Reinoso, F.: Effect of the porous structure in carbon materials for CO2 capture at atmospheric and high-pressure. Carbon **67**, 230–235 (2014). https://doi.org/10.1016/j.carbon.2013.09.086